Chinese Journal of Polymer Science Vol. 31, No. 1, (2013), 98–109

Chinese Journal of Polymer Science
© Chinese Chemical Society
Institute of Chemistry, CAS
Springer-Verlag Berlin Heidelberg 2013

OSCILLATORY SHEAR-ACCELERATED EXFOLIATION OF GRAPHITE IN POLYPROPYLENE MELT DURING INJECTION MOLDING*

Nan Li, Wei Cheng, Kun Ren, Feng Luo, Ke Wang** and Qiang Fu**
College of Polymer Science and Engineering, State Key Laboratory of Polymer Materials Engineering, Sichuan University, Chengdu 610065, China

Abstract In this study, good dispersion status of graphite in a nonpolar, intractable polymer, *i.e*. polypropylene (PP), was realized in melt processing by using a specific dynamic packing injection molding (DPIM) technique. The exfoliation extent of graphite increased remarkably from the skin zone to the core zone of the molded part, as confirmed by combination of WAXD, SEM and TEM analyses, indicating an accelerated exfoliation occurred during the DPIM processing. This phenomenon is due to decreased melt flow channel and increased melt viscosity as the solidification takes place from the wall into the center, which leads to greatly increased shear force. The good dispersion of graphite results in obvious reinforcements of both tensile strength and impact strength by adding moderate amount of graphite. The present study proposes a promising route for realizing the large-scale fabrication of structural parts of polymer/exfoliated-graphite nanocomposites with excellent mechanical properties.

Keywords: Polymer-matrix composites; Mechanical properties; Injection moulding.

INTRODUCTION

Graphene was discovered by Geim *et al*.[1] who used micromechanical method to exfoliate graphite into two-dimensional atomically-thick single sheet with carbon atoms arranged in a honeycomb lattice. Particularly, single atom-layer graphene is the strongest material ever measured[2], and can serve as mechanical modifier for polymer materials. So far, most of polymer-graphene hybrids were fabricated by using chemically or thermally pretreated graphites, *e.g*., graphite oxide (GO)[3–5], expanded graphite[6–11] and thermally exfoliated graphite oxide (TEGO)[12–16]. Even with pretreatment, the fabrication of polymer/graphite nanocomposites *via* conventional melt processing is still a challenging issue due to thermodynamic and/or kinetic limitations, often leading to limited property enhancement. Several studies reported melt mixing processes using TEGO[17] and/or graphene nanoplatelets (GNPs)[18–21] as filler, where these fillers could be fed directly into extruder and dispersed into polymer matrix without the use of any solvents or surfactants. Kim *et al*.[22, 23] successfully prepared two kinds of exfoliated graphite/polymer nanocomposites by simple melt processing. In their works polar polymers such as polycarbonate and polyester were adopted as basal resin. Recently, Wakabayashi *et al*.[24] had fabricated polypropylene-graphite nanocomposites associated with conventional processing through a so-called solid-state shear pulverization (SSSP) technique. The tensile strength and modulus of the nanocomposites had an obvious improvement, but the impact strength decreased severely.

In our previous work, a specific processing technique, dynamic packing injection molding (DPIM), had

* The work was financially supported by the National Natural Science Foundation of China (No. 21074075) and the program for the new century excellent talents of ministry of education of China (NCET-11-0348).
** Corresponding authors: Ke Wang (王柯), wkestar@scu.edu.cn
Qiang Fu (傅强), E-mail: qiangfu@scu.edu.cn
Received May 9, 2012; Revised July 9, 2012; Accepted July 25, 2012
doi: 10.1007/s10118-013-1204-0

been utilized to fabricate exfoliated polypropylene (PP)/organoclay nanocomposite[25]. The DPIM equipment can offer oscillatory shear field, which forces composite melt to move repeatedly during the solidification process (cooling) in the mold chamber. Strong shear stress induced high level of exfoliation of organoclay in the core zone of molded part[26]. Since graphite also belongs to layered substance and its primary units are consisted of graphite thin-sheets, which are stacking together in a layer-by-layer fashion, we attempt to directly exfoliate graphite tactoids in PP melt by using the DPIM technique, thereby to attain exfoliated graphite/PP nanocomposite. The whole fabrication process involves no oxidation/reduction or functionalization procedure. So the approach proposed in this study is convenient and high effective. Our present paper is organized as follows. First, careful structural characterizations of graphite dispersion status is performed from skin zone to core zone along the sample thickness in the injection-molded part of high molecular weight polypropylene (HPP)/graphite composites. Second, the mechanical properties of the injection-molded parts of HPP/graphite composites are estimated and discussed. Finally, a possible schematic of exfoliation mechanism is illustrated. For a comparative purpose, another low molecular weight polypropylene (LPP) is also introduced. A comparative analysis between the cases of utilizing HPP or LPP as basal resin emphasizes that strong shear stress might play a crucial role for inducing the high extent of graphite exfoliation.

EXPERIMENTAL

Materials

Two commercially available isotactic polypropylenes (*i*PP), with melt flow index of 3 g/10min (230°C, 2.16 kg loading) and 15 g/10min, were adopted as high molecular weight PP (HPP) and low molecular weight PP (LPP), respectively. Graphite was in powder form with mesh size of 40 micrometer and density of 2.86 g/cm^3.

Sample Preparation

HPP/graphite and LPP/graphite (0 wt%, 1 wt%, 3 wt%, 5 wt%, 10 wt%, 20 wt%) composites were melt-mixed in a TSSJ-25 co-rotating twin-screw extruder. After the pelletizing and drying processes, the pellets of composites were injected into a mold with the aid of an SZ 100 g injection molding machine. At the same time, DPIM technology was applied to introduce oscillatory shear field on cooling melt during the packing stage by two pistons that moved repeatedly with the same frequency (1.0 Hz). The processing parameters, the characteristics and detailed experimental procedure of DPIM, and the geometrical sizes of molded bar were described in Refs[27, 28]. We also carried out injection molding by using the same processing parameters but without shearing for comparison purpose. The specimen obtained by DPIM was called dynamic sample, while the specimen obtained by conventional injection molding was called static sample.

Characterization

Wide-angle X-ray diffraction (WAXD) measurements were conducted by a Panalytical X'pert PRO diffractometer in reflection mode. The scanning 2θ range was 10°–30° with a scanning rate of 2 (°)/min.

The 2D wide-angle X-ray diffraction (2D-WAXD) experiments were conducted on a Bruker D8 Discover diffractometer with a general area detector or a diffraction system (GADDS) as a detector. The two-dimensional diffraction patterns were recorded in a transmission mode at room temperature. The wavelength of the monochromatic X-ray from Cu Kα radiation was 0.154 nm. The samples were placed with the orientation (flow direction) perpendicular to the projection beams. The backgrounds of all the 2D WAXD patterns had been extracted, thus allowing a qualitative comparison between various samples. The orientation level of various planes could be calculated by the order parameter *f*, which was calculated as following:

$$f = \frac{3 < \cos^2 \varphi > -1}{2} \tag{1}$$

$$< \cos^2 \varphi >= \frac{\int_0^{\frac{\pi}{2}} I(\phi) \sin\phi \cos^2\phi \mathrm{d}\phi}{\int_0^{\frac{\pi}{2}} I(\phi) \sin\phi \mathrm{d}\phi} \tag{2}$$

where φ is the angle between the normal of a given (hkl) crystal plane and the shear flow direction, and I is intensity. Its limiting values of order parameter f, taking $\varphi = 0$ as the shear flow direction, are −0.5 for a perfect perpendicular orientation and 1.0 for a perfect parallel orientation. A random, disordered state gives $f = 0$.

Microscopic morphology observations were conducted on a Hitachi S3400 + EDX scanning electron microscopy (SEM) under an acceleration voltage of 20 kV. The molded parts were fractured along the direction perpendicular to the flow direction in liquid nitrogen. Transmission electron microscopy (TEM) experiments were performed on a JEM-100 CX TEM instrument under an acceleration voltage of 80 kV.

The notched Izod impact strength experiments were tested with a VJ-40 izod machine according to ASTM D 256-04 standard. Tensile tests were performed using a SANS universal testing machine (Shenzhen, China), performed upon a crosshead speed of 2 mm/min, according to ASTM D 638-03 standard.

Dynamic mechanical analysis (DMA) was performed using a DMA Q800 instrument (TA Instruments). The whole part specimens (including dynamic and static parts) with the dimensions of 40 mm × 6 mm × 3.5 mm (length × width × thickness) were heated from −40°C to 120°C at a heating rate of 3 K/min. The experiments were conducted in three-point bending mode under a frequency of 1 Hz.

RESULTS AND DISCUSSION

WAXD Analysis of Injection-molded Parts of HPP/Graphite Composites

The schematic model of DPIM equipment is plotted as Fig. 1(a). Two pistons 3 and 9 move repeatedly with a fixed frequency of 1 Hz to induce the mobility of composite melt in mold chamber 6. Meanwhile, the solidification (cooling) of melt occurs gradually from the wall to the center of mold, resulting in macroscopic multi-layer structure in the as-prepared injection-molding parts, as sketchily represented in Fig. 1(b). The skin zone begins from the outmost surface to the depth of about 200 μm, the intermediate zone ranges from 200 μm to 1200 μm, and the core zone varies from 1200 μm to the center of the injection part (1750 μm).

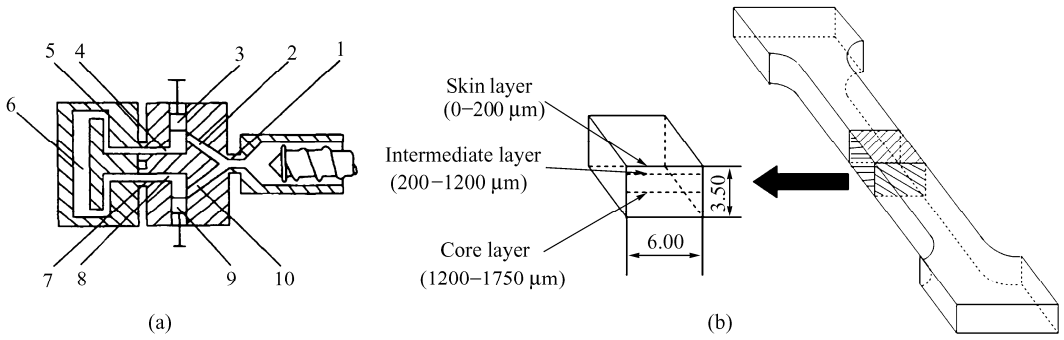


Fig. 1 (a) Schematic illustration of dynamic packing injection molding equipment: (1) nozzle, (2) sprue A, (3) piston A, (4) runner A, (5) connector, (6) specimen, (7) connector, (8) runner B, (9) piston B, (10) sprue B; (b) Geometric profile of as-prepared injection-molding part

The dispersion and exfoliation statuses of graphite at different zones of the dynamic part of HPP/graphite (3 wt%) composite have been estimated by WAXD measurements, the corresponding WAXD patterns are shown in Fig. 2(a). From the skin zone pattern, a sharp diffraction peak at $2\theta = 26.6°$ is corresponding to tactoid of graphite, which indicates an inter-layer spacing of about 0.34 nm. Afterwards, with increasing the depth of the dynamic part, the intensity of this characteristic peak becomes weaker and weaker, a dramatic decrease of intensity occurs within the depth region from 50 μm to 400 μm, which implies that there may exist exfoliated

graphite in composites and exfoliation degree increases gradually with the depth of the dynamic part. Particularly, the profile of this diffraction peak is difficult to be detected after the depth of 1200 μm, maybe it represents a complete exfoliation of graphite. Similar phenomenon can also be seen on the composite with 10 wt% graphite (Fig. 2b). But compared with the composites with low graphite content (3 wt%), the characteristic diffraction peak of graphite tactoid can still be observed at the core layer of about 1700 μm. So it suggests that, this oscillatory shear field is limited to the exfoliation of graphite when the graphite content is relatively high (10 wt%). Similar results are also reported in Ref. [30]. Compared with the results reported by Wakabayashi *et al*.[30], our results can better reflect that hierarchical structure raises different exfoliation level of graphite from skin to core layer of injection molded parts. Based on the above facts, one may argue that graphite substance migrating to or selectively distributing in the surface zones of molded part can also induce this phenomenon. However, the thermogravimetric analysis (TGA) result of the composite with 3 wt% graphite indicates that the mass fractions of final residual ash at different zones are all approximately the same of around 3 wt%. This result confirms that the disappearance of characteristic peak in the inner zones is due to the exfoliation of graphite. In addition, it is also noted that the peak location of graphite reflection doesn't vary at all within the whole molded part, which implies that no intercalation of PP chains into the gallery of graphite tactoid occurred during the DPIM process. The exfoliation mode is most like to the finding on PP/organoclay nanocomposite[26] that more and more thin sheets were peeled away from the edge of graphite tactoid from the skin zone to the core zone.

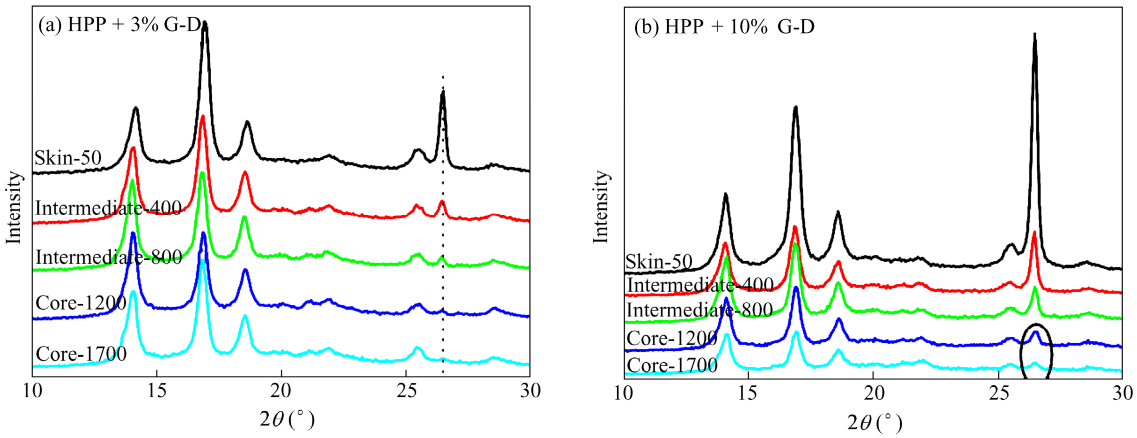


Fig. 2 Evolution of WAXD pattern along the depth of dynamic samples for HPP/graphite composites with (a) 3 wt% and (b) 10 wt% graphite

Electron Microphotographs of Injection-molded Parts of HPP/Graphite Composites

The dispersion status and exfoliation level of graphite substance in molded part have been visually characterized by SEM experiments. The SEM microphotographs for different zones in dynamic samples of nanocomposites with 3 wt% and 10 wt% graphite are shown in Fig. 3 and Fig. 4. For the composite with 3 wt% graphite, block agglomerate-granules of graphite, with large size of more than 10 μm, are found in the skin layer of dynamic molded part. This size is a little smaller than that of the original graphite as shown in Fig. 5, it's mainly due to scattering of graphite aggregates during molten extrusion blending process. However, obviously improved-dispersion of graphite can be seen in the intermediate layer and core layer. This good dispersion state is embodied in both the reduced lateral size and thickness. Particularly, we can note that in the core zones, most of graphite is exfoliated into less than one hundred nanometers in thickness and the lateral size decreases severely. At higher magnification observation, the exfoliated graphite exists in the form of nano-thin-sheets. It is because of strong shear force resulted from reciprocating moving of the composite melt during the solidification process of injection molding parts in the mold chamber. As to the composite with 10 wt% graphite, the dispersion of graphite also becomes better and better, and lateral sizes and thickness of graphite substance get smaller and smaller from skin to core layer (Fig. 4). However, compared to the composite with 3 wt% graphite, the

exfoliation extent of graphite in corresponding layer is relatively incomplete and the thickness is bigger, which is accordance with the results of WAXD.

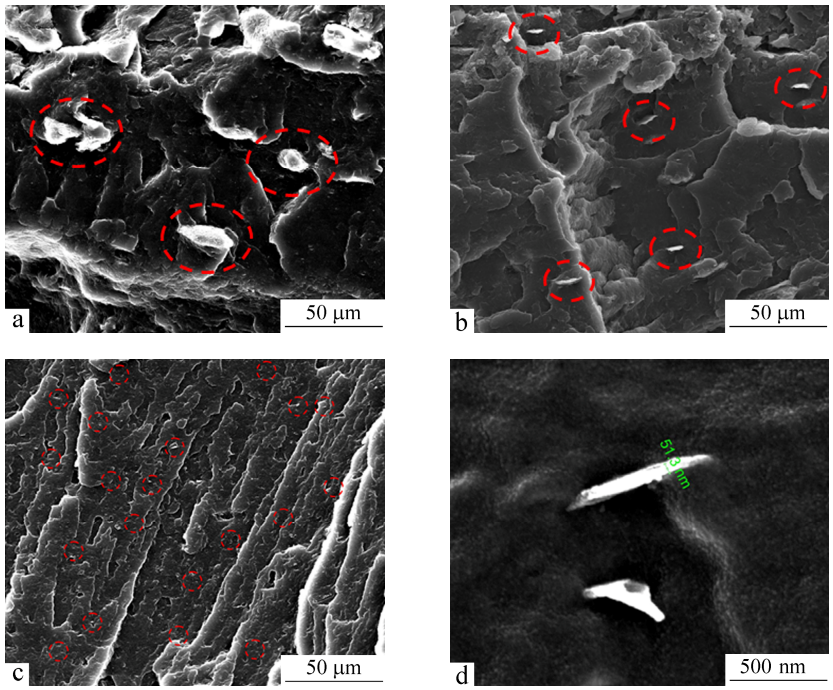


Fig. 3 SEM microphotographs of dynamic samples of HPP/graphite composites with 3 wt% graphite: (a) the skin layer, (b) the intermediate layer, (c) the core layer and (d) the amplification of (c)

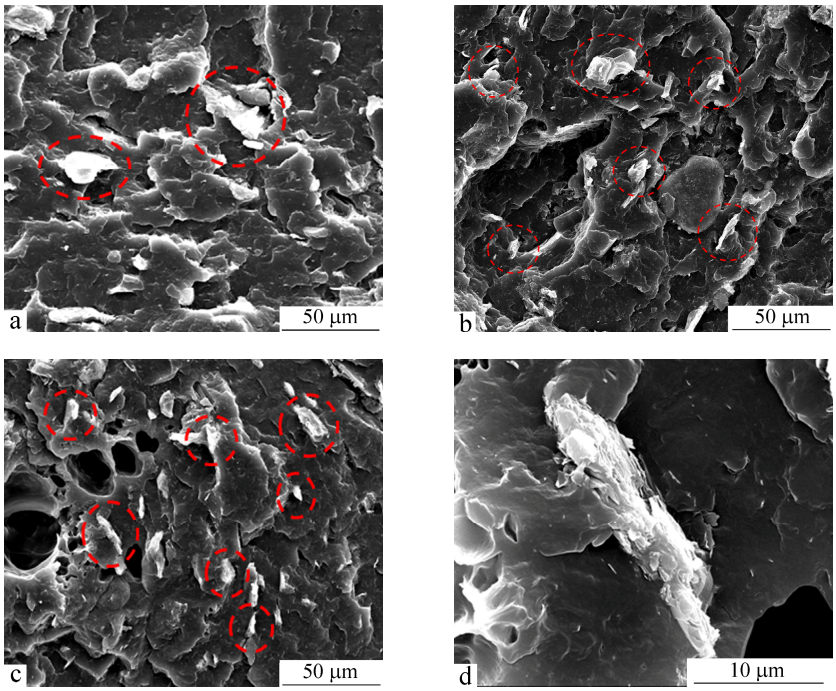


Fig. 4 SEM microphotographs of dynamic samples of HPP/graphite composites with 10 wt% graphite: (a) the skin layer, (b) the intermediate layer, (c) the core layer and (d) the amplification of (c)

An exact observation of the exfoliation morphology of graphite tactoids in the composite with 3 wt% graphite has been done by using TEM. Overall, by shear the graphite can disperse well in the core layer of dynamic molded part, as shown in Fig. 6, which is consistent with the SEM results. Moreover, it can be observed that most of graphite substances have been exfoliated into nano-scale sheets (light black areas in Fig. 6) and only a few aggregates of graphite (dark black areas in Fig. 6) can be observed. This can better explain why the intensity of characteristic diffraction peak of graphite tactoid at the core layer is so weak.

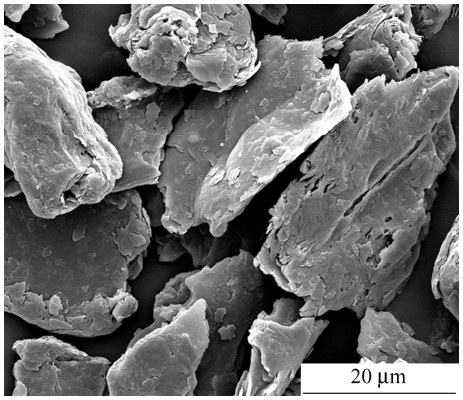


Fig. 5 Microphotograph of original graphite

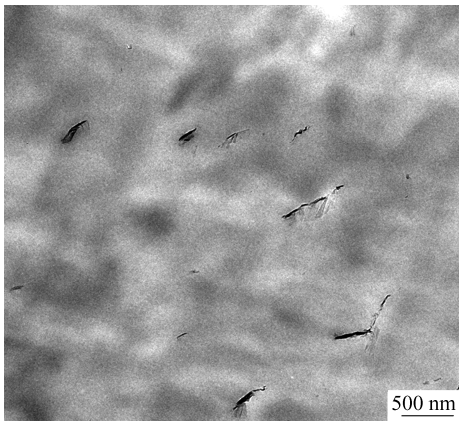


Fig. 6 TEM microphotographs of the core zone of dynamic samples for HPP/graphite composite with 3 wt% graphite

By a combination of WAXD, SEM and TEM, a schematic representation of the evolution of dispersion morphology in the injection part from skin to core layer has been sketched in Fig. 7. The dispersion morphology of graphite substance experiences a three-stage development in the DPIM process: (1) At the skin zone, relatively large graphite blocks with tens of micrometers in size were maintained; (2) Block granules were broken up into platelet-shaped graphite tactoids with high aspect ratio, and few thin sheets were peeled from the edge of graphite tacoids at the intermediate zone; (3) Finally, at the core zone, platelet-shaped graphite tactoids are further broken into smaller pieces under shear field and most blocky graphite tactoids are exfoliated into nano-scale thin sheets with tens of nanometers in thickness.

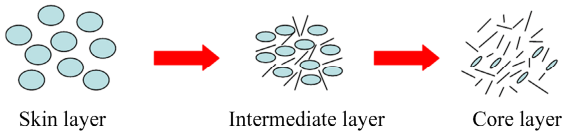


Fig. 7 Schematic representation of exfoliation process of graphite in melt shear field during the DPIM process

Mechanical Enhancements in Injection-molded Parts of HPP/Graphite Composites

Subsequently, the mechanical properties for static and dynamic molded parts are illustrated in Fig. 8 as a function of graphite content. It is noteworthy that a dramatic increment of impact toughness is achieved for the dynamic parts. When the graphite is increased to 3 wt%, the impact strength is improved by 147% (from 8.5 kJ/m^2 to 20.5 kJ/m^2). This is because of good dispersion state of graphite induced by oscillatory shear field during DPIM when the graphite content is 3 wt%. After this point, the impact strength is depressed rapidly. From the results of SEM, it is due to seriously aggregation of graphite occurring in the molded part even if the DPIM equipment has been utilized. For static molded parts, the impact strength is almost unchanged within the entire graphite content range, corresponding unchanged structure of graphite tactoid in the conventional injection molding processing. As for tensile strength, about a 10% increment is available for both static and dynamic molded parts containing 3 wt% graphite, however, this range of increase is relatively low, we think that maybe the original graphite used here is relatively small in size and becomes much smaller after oscillatory shear, the fracture way of the nanocomposites is the "pull-out", which depends on the higher interaction between matrix and fillers for the increasing tensile strength of the nanocomposites[29]. Nevertheless, our results indicate that a composite with excellent comprehensive mechanical properties has been successfully prepared by this processing method.

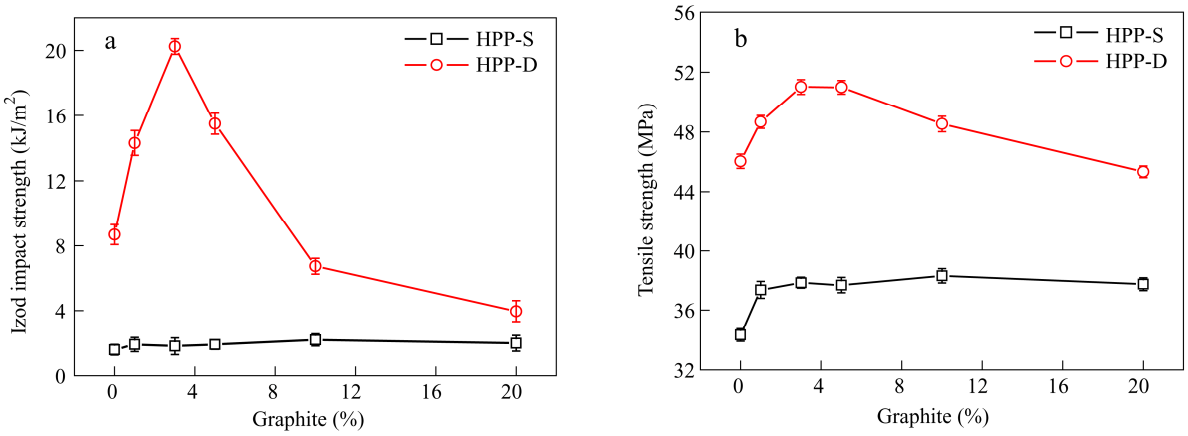


Fig. 8 (a) Impact strength and (b) tensile strength of static and dynamic samples for HPP/graphite composites as a function of graphite content

To further estimate the mechanical properties of composites, DMA measurements have also been adopted. The DMA curves of storage modulus versus temperature for the injection parts of neat PP and composites are presented in Fig. 9. In general, the storage modulus for the dynamic samples is higher than that for the static counterparts during the whole experimental temperature range. It's because of the higher orientation level induced by shear for dynamic samples, which is in agreement with the results of impact strength and tensile strength. For static samples, the higher the graphite content, the larger the mechanical modulus is, and this magnitude of reinforcement is great when the testing temperature is below T_g, but it becomes small when the testing temperature is above T_g, indicating that graphite could restrict the movement of molecular chains and result in the increased damping force for the motion of molecules. For static samples the storage modulus

increases by about 8% (from 3585 MPa to 3871 MPa) and 13% (from 3585 MPa to 4064 MPa) at –40°C when the graphite contents are 3 wt% and 10 wt% respectively; for dynamic samples, when the temperature is at –40°C, a greater increasing of about 12% (4300 MPa to 4826 MPa) and 32% (4300 MPa to 5665 MPa) can be observed when the graphite contents are 3 wt% and 10 wt% respectively. We suppose, this is because more graphite sheets are exfoliated apart from original graphite under shear, which can result in a greater increasing for the storage modulus. Generally speaking, the special processing method of DPIM can effectively improve the dispersion of graphite in nanocomposites.

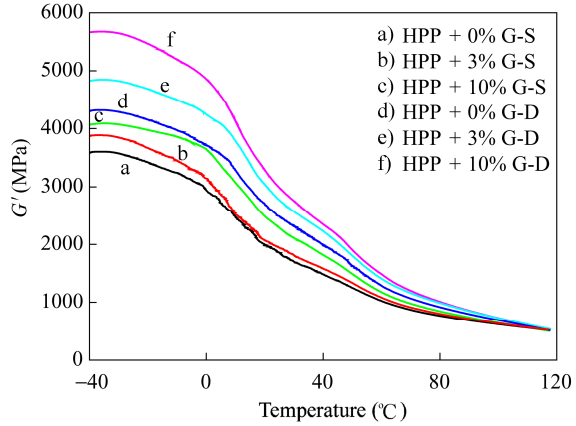


Fig. 9 Storage modulus of static and dynamic samples for HPP/graphite composites with different graphite contents as a function of temperature

The Effect of Graphite on the Orientation Level of iPP Matrix

To assess the influence of graphite on the orientation of *i*PP, 2D-WAXD measurements have been implemented, and the resulted patterns are shown in Fig. 10 and the calculated orientation degrees are listed in Table 1. Even 3 wt% and/or 10 wt% graphite is added, the orientation degrees of *i*PP are almost constant in every tested layer. It is due to that oscillatory shear field restrains the relaxation of oriented molecular chains in the whole molded parts during the packing stage. And the mechanical properties are independent on the matrix orientation.

Table 1. Orientation parameters of (040) plane of *i*PP at the different layers of various molded bars

	HPP + 0% G-D	HPP + 3% G-D	HPP + 10% G-D
Skin	0.56	0.50	0.49
Intermediate	0.55	0.52	0.56
Core	0.55	0.54	0.52

Mechanism of Oscillatory Shear-induced Accelerated Exfoliation

The reason for the occurrence of accelerated exfoliation in the inner zones of DPIM part is that the shear stress in composite melt was enhanced dramatically as the melt solidification proceeded from skin to core. A simple relationship between shear stress (τ), melt viscosity (η) and shear velocity ($\dot{\gamma}$) is expressed as:

$$\tau = \eta \cdot \dot{\gamma} = \eta \cdot \frac{\mathrm{d}\upsilon}{\mathrm{d}Y} \tag{3}$$

where υ is melt flow speed and Y is thickness of melt region. With the proceeding of melt solidification, the melt temperature decreased continuously, leading to a dramatic increment in viscosity, especially at the latter stage of solidification. On the other hand, as schematically indicated in Fig. 11, the melt solidification during DPIM process was accompanying with the repeated flowing of melt under certain fixed flow speed (υ). With the solidification front progressed to the center of mold chamber, the cross-section area for melt flow might gradually decrease. Namely, Y became narrow, resulting in a high shear velocity. Since both of η and $\dot{\gamma}$ all

improved remarkably at the latter stage of DPIM process, ultrahigh shear stress was expected when the melt solidification proceeded to the core zone and finally induced highly exfoliated morphology at this zone of injection part.

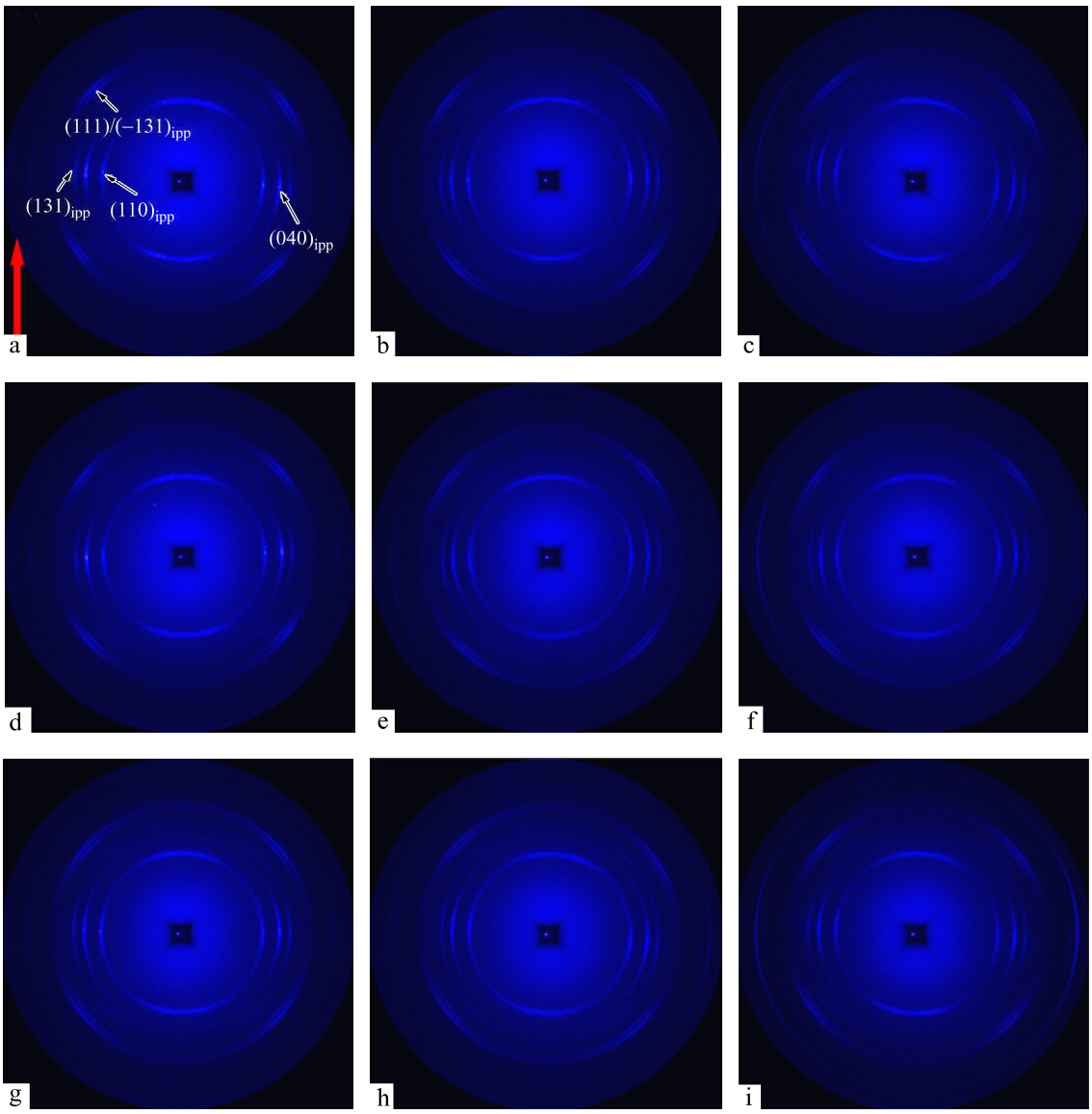


Fig. 10 2D-WAXS patterns of the skin layers of injection-molded bars: (a) pure *i*PP, (b) PP-3G-D and (c) PP-10G-D; of the intermediate layers of injection-molded bars: (d) pure *i*PP, (e) PP-3G-D and (f) PP-10G-D; of the core layers of injection-molded bars: (g) pure *i*PP, (h) PP-3G-D and (i) PP-10G-D (The shearing direction is vertical as shown by the arrow.)

To further validate if strong shear stress is favorable for realizing the accelerated exfoliation of graphite, the exfoliation extent in the DPIM part of composite containing low molecular weight *i*PP (LPP) was also ascertained. The using of LPP might reduce melt viscosity (η) and thus induce lower shear stress (τ), as compared to the case of using high molecular weight *i*PP (HPP). By comparing the WAXD patterns (Fig. 12) for the core zones (about at the 1700 μm depth) of HPP/graphite and LPP/graphite composites, the characteristic diffraction peak of graphite is appreciable for LPP matrix; meanwhile, a typical morphology of thinner tactoid of

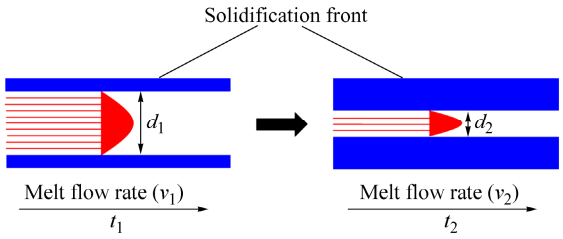


Fig. 11 Schematic mechanism of shear velocity increased during the DPIM process

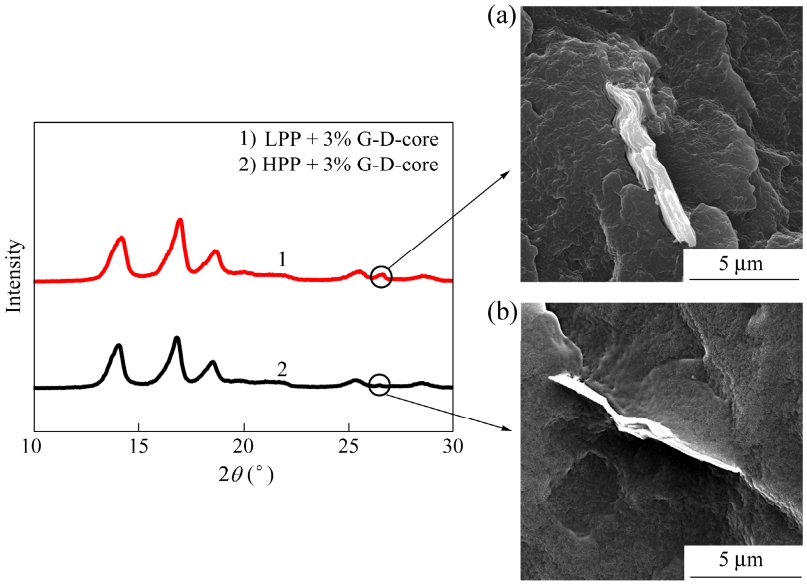


Fig. 12 Dispersion of graphite tactoids at the core zones of dynamic samples for (a) LPP/graphite composite and (b) HPP/graphite composite with 3 wt% graphite

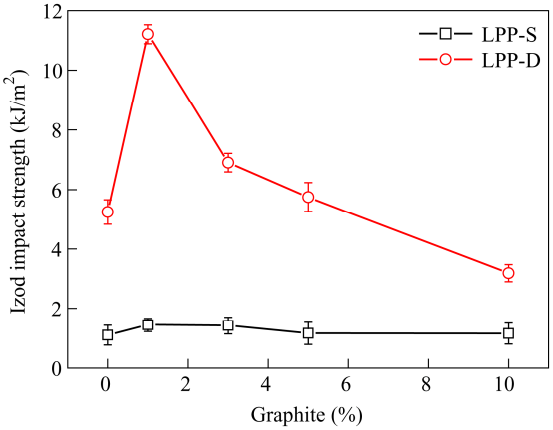


Fig. 13 Impact strength of static and dynamic samples for LPP/graphite composites as a function of graphite content

graphite is found for HPP/graphite composite (Fig. 12b), indicating a higher extent exfoliation in HPP/graphite composite than that in LPP/graphite composite. The trend of impact strength versus graphite content for LPP/graphite composites, as shown in Fig. 13, is similar to that for HPP/graphite composites: there exists a

maximum when a certain low content of graphite (1 wt%) was added, and it subsequently decreases with further increasing graphite content. However, the optimized increment in toughness for LPP/graphite composite is about 100%, which is lower than the case of HPP/graphite composite (147%). Obviously, this is due to relatively low exfoliation extent of graphite in LPP/graphite composite, as confirmed by Fig. 12. So, by a comparative analysis between HPP and LPP, it is suggested that strong shear stress plays a crucial role in inducing the good dispersion of graphite in the injection-molded parts of composites.

CONCLUSIONS

In summary, oscillatory shear is an effective pathway to induce good dispersion of graphite in PP matrix. By using DPIM technique, high exfoliation extent of PP/graphite nanocomposite can be realized readily in the inner region of injection part. The graphite tactoids are exfoliated as a fashion that thin sheets are peeled away from their edges, layer-by-layer. The efficiently promoted dispersion brings the increment of mechanical property, particularly, a prominent improvement in impact toughness. In addition, strong shear stress is crucial for achieving highly exfoliated morphology during polymer/graphite composite molding processing. As we know, chemical compatibility is another important factor to dominate the dispersion behavior of inorganic filler in polymer-based composite. So some pre-treatments for tailoring/improving interfacial interaction between graphite sheets and PP matrix will be implemented before the melt injection-molding step in our future work, and extremely high extent of graphite exfoliation is desired *via* a synergetic effect of chemical compatibility and physical shearing.

REFERENCES

1 Novoselov, K.S., Geim, A.K., Morozov, S.V., Jiang, D., Zhang, Y., Dubonos, S.V., Grigorieva, I.V. and Firsov, A.A., Science, 2004, 306: 666
2 Lee, C., Wei, X., Kysar, J.W. and Hone, J., Science, 2008, 321: 385
3 Stankovich, S., Dikin, D.A., Dommett, G.H.B., Kohlhaas, K.M., Zimney, E.J., Stach, E.A., Piner, R.D., Nguyen, S.T. and Ruoff, R.S., Nature, 2006, 442: 282
4 Ramanathan, T., Stankovich, S., Dikin, D.A., Liu, H., Shen, H., Nguyen, S.T. and Brinson, L.C., J. Polym. Sci. Part B, 2007, 45: 2097
5 Mack, J.J., Viculis, L.M., Ali, A., Luoh, R., Yang, G., Hahn, H.T., Ko, F.K. and Kaner, R.B., Adv. Mater., 2005, 17: 77
6 Wang, W.P., Liu, Y., Li, X.X. and You, Y.Z., J. Appl. Polym. Sci., 2006, 100: 1427
7 Cho, D., Lee, S., Yang, G., Fukushima, H. and Drzal, L.T., Macromol. Mater. Eng., 2005, 290: 179
8 Du, X.S., Xiao, M. and Meng, Y.Z., Eur. Polym. J., 2004, 40: 1489
9 Zheng, W., Wong, S.C. and Sue, H.J., Polymer, 2002, 43: 6767
10 Yasmin, A, Luo, J.J., Daniel, I.M., Compos. Sci. Technol., 2006, 66: 1182
11 Uhl, F.M., Yao, Q., Nakajima, H., Manias, E. and Wilkie, C.A., Polym. Degrad. Stab., 2005, 89: 70
12 Chen, G.H., Wu, D.J., Weng, W.G. and Yan, W.L., J. Appl. Polym. Sci., 2001, 82: 2506
13 Xiao, P., Xiao, M. and Gong, K., Polymer, 2001, 42: 4813
14 Pan, Y.X., Yu, Z.Z., Ou, Y.C. and Hu, G.H., J. Polym. Sci. Part B, 2000, 38: 1626
15 Schniepp, H.C., Li, J.L., McAllister, M.J., Sai, H., Herrera-Alonso, M., Adamson, D.H., Prud'homme, R.K., Car, R., Saville, D.A. and Aksay, I.A., J. Phys. Chem. B, 2006, 110: 8535
16 Kotov, N.A., Dékány, I. and Fendler, J.H., Adv. Mater., 1996, 8: 637
17 Zhang, H.B., Zheng, W.G., Yan, Q., Yang, Y., Wang, J.W., Lu, Z.H., Ji, G.Y. and Yu, Z.Z., Polymer, 2010, 51: 1191
18 Kim, I.H. and Jeong, Y.G., J. Polym. Sci. Part B, 2010, 48: 850
19 Jiang, X. and Drzal, L.T., Polym. Compos., 2010, 31: 1091
20 Kim, S., Do, I. and Drzal, L.T., Polym. Compos., 2010, 31: 755

21 Kalaitzidou, K., Fukushima, H. and Drzal, L.T., Compos. Sci. Technol., 2007, 67: 2045
22 Kim, H. and Macosko, C.W., Polymer, 2009, 50: 3797
23 Kim, H. and Macosko, C.W., Macromolecules, 2008, 41: 3317
24 Wakabayashi, K., Pierre, C., Dikin, D.A., Ruoff, R.S., Ramanathan, T., Brinson, L.C. and Torkelson, J.M., Macromolecules, 2008, 41: 1905
25 Zhang, Q., Wang, Y. and Fu, Q., J. Polym. Sci. Part B, 2003, 41: 1
26 Wang, K., Liang, S., Zhang, Q., Du, R. and Fu, Q., J. Polym. Sci. Part B, 2005, 43: 2005
27 Liang, S., Wang, K., Yang, H., Zhang, Q., Du, R. and Fu, Q., Polymer, 2006, 47: 7115
28 Wang, K., Liang, S., Du, R., Zhang, Q. and Fu, Q., Polymer, 2004, 45: 7953
29 Blighe, F.M., Young, K., Vilatela, J.J., Windle, A.H., Kinloch, I.A., Deng, L., Young, R.J. and Coleman, J.N., Adv. Funct. Mater., 2011, 21: 364
30 Wakabayashi, K., Brunner, P.J., Masuda, J., Hewlett, S.A. and Torkelson, J.M., Polymer, 2010, 51: 5525